Post-Print

This is the accepted version of:

Probing the Impact of the Initiator Layer on Grafted-from Polymer Brushes: A Positron Annihilation Spectroscopy Study

Guido Panzarasa,*,[†][ID] Stefano Aghion,[‡,§] Gianluigi Marra,[‖] Andreas Wagner,[⊥] Maciej Oskar Liedke,[⊥] Mohamed Elsayed,[#] Reinhard Krause-Rehberg,[#] Rafael Ferragut,[‡,§] and Giovanni Consolati*,[%]

[†]Department of Polymer Engineering and Science, Montanuniversität, Otto-Glöckel Straße 2, 8700 Leoben, Austria

[‡]LNESS, Department of Physics, Politecnico di Milano, via Anzani 42, 22100 Como, Italy

[§]Istituto Nazionale di Fisica Nucleare, via Celoria 16, 20133 Milano, Italy

[‖]Eni Donegani Research Center for Renewable Energies and Environment, Via Fauser 4, 28100 Novara, Italy

[⊥]Institute of Radiation Physics, Helmholtz-Zentrum Dresden-Rossendorf, Bautzner Landstraße 400, 01328 Dresden, Germany

[#]Institut für Physik, Martin-Luther-Universität Halle, 06099 Halle, Germany

[%]Department of Aerospace Science and Technology, Politecnico di Milano, via La Masa 34, 20156 Milano, Italy

ABSTRACT: Grafting-from is the technique of choice to obtain polymer brushes. It is based on the growth of polymer chains directly from an initiator-functionalized surface, and its development gained momentum thanks to recent advances in controlled polymerization techniques. However, despite the great amount of work that has been performed on this subject, the influence exerted by the initiator layer on the characteristics of the resulting brushes has been almost completely overlooked. Our group has already demonstrated that positron annihilation spectroscopy (PAS) is a valuable analytical tool for the study of polymer brushes. Here, we applied this technique to show that differences in the organization of the initiator layer dramatically reflect on the characteristics of polymer brushes. Brushes made by surface-initiated atom transfer radical polymerization (ATRP) of a pH-responsive polymer, poly(dimethylaminoethyl methacrylate) (PDMAEMA), were investigated also in terms of the effects of protonation and of the incorporation of silver nanoparticles inside the brushes, shining a new light on the internal structure of such complex, fascinating systems.
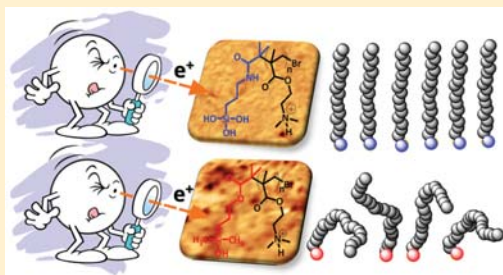
■ INTRODUCTION

In recent years, positron annihilation spectroscopy (PAS) has gained increasing visibility in the polymer research field,[1,2] an interest justified by its great potentialities for the study of thin and ultrathin polymer films. Positron (e^+), the antiparticle of the electron, and its bound state positronium (Ps) are uniquely sensitive to pores and cavities where they tend to localize, and their annihilation profiles can give precious information about their chemical environment.[3] The sensitivity of PAS to interface phenomena makes it powerful to investigate glass transition temperature, multilayer structures, and the distribution of particles in composites. However, PAS has much to give to polymer science: its applications extend not only to fundamental studies but also to disciplines closely related to polymer science such as nanotechnology, membranes, sensors, and biomedicine. Polymer brushes, being at the cutting edge of all of these fields,[4−9] are a perfect playground to demonstrate the potentialities of PAS.

Our group has been the first to report the application of PAS for the study of the pH-responsive behavior and nanoparticle incorporation of polymer brushes.[10] Here, our goal is to investigate, by means of PAS, the structural differences in grafted-from polymer brushes that arise from the initiator layer. Two different PAS techniques have been adopted: (i) the Doppler broadening spectroscopy (DBS) of annihilation radiation, in which the broadening of the 511 keV peak coming from the positron−electron annihilations is measured, performed at the VEPAS laboratory in Como, and (ii) positron annihilation lifetime spectroscopy (PALS), which measures the positron and Ps lifetime implanted in a sample material, carried out at the ELBE at HZDR in Dresden. Both in the DBS and PALS techniques, positrons are implanted with a controlled kinetic energy into the studied material and annihilate either as free positrons with the electrons in two 511 keV γ-rays or in the form of positronium. Ps exists in the ground state in two sublevels: singlet (para-Ps, p-Ps) and triplet (ortho-Ps, o-Ps), depending on the spins of the electron and positron (antiparallel or parallel, respectively). In vacuum, their lifetimes are very different (0.125 and 142 ns for p-Ps and o-Ps, respectively), and this is true also for their annihilation features:
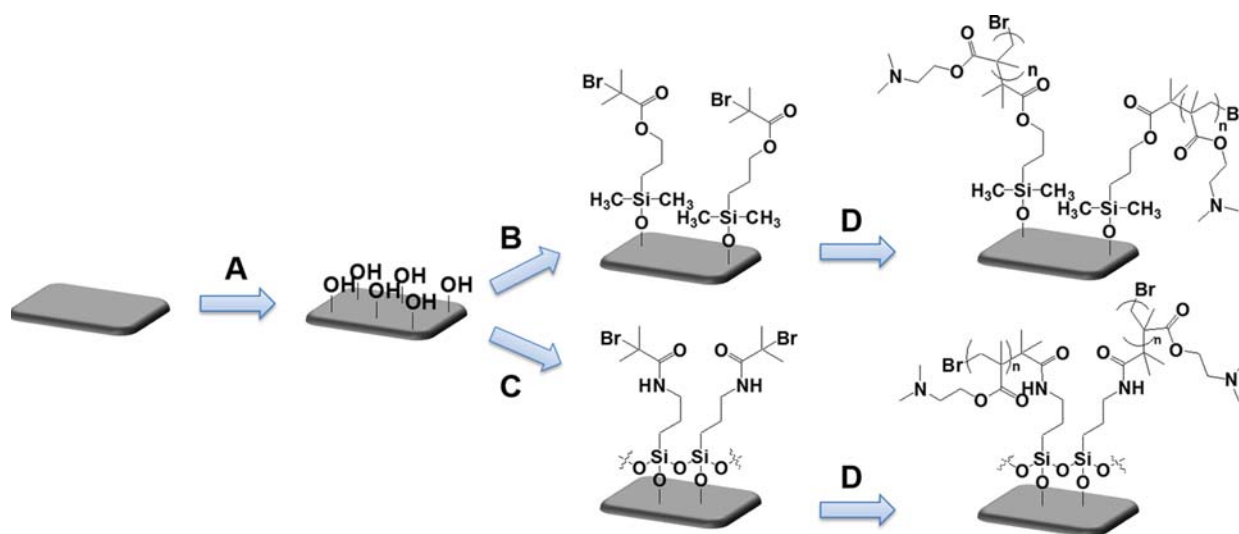
Figure 1. Synthesis of PDMAEMA brushes by surface-initiated ATRP using two different initiators. The substrate is silicon wafer with native oxide. (A) conc H_2SO_4/conc H_2O_2 3:1 v/v, 100 °C, 1 h; (B) anhydrous toluene, BIB-DMES 10 mM, 55 °C, 4 h then 30 °C overnight; (C) anhydrous toluene, BIB-APTES 10 mM, 55 °C, 4 h then 30 °C overnight. (D) DMAEMA, CuBr, bipyridyl, MeOH/H_2O 4:1 v/v, 30 °C.

67 p-Ps annihilates with emission of two γ-rays (511 keV each),
68 while o-Ps annihilates by emitting three γ-rays, producing a
69 continuous energy distribution for each photon between 0 and
70 511 keV, where the energy sum of the three photons of the o-
71 Ps annihilation is 1022 keV. When o-Ps is formed inside a
72 cavity of a material (such as a free volume hole in a polymer, a
73 cage in a zeolite, a pore in a porous medium), the three-γ
74 annihilation probability is reduced by the pick-off effect; that is,
75 the positron of the o-Ps may annihilate with an electron of the
76 cavity surface in a relative singlet state with emission of two γ-
77 rays instead of three. As has been demonstrated, Ps forms into
78 the free volumes of many polymers and PAS can detect buried,
79 isolated pores of 0.2−50 nm size, which are not accessible to
80 conventional probes.[11,12]

81 We focused on grafted-from brushes made of poly(dimethyl-
82 aminoethyl methacrylate) (PDMAEMA), a well-known pH-
83 responsive polymer with applications spanning from the
84 development of sensors to gene delivery.[13−15] PDMAEMA
85 brushes were obtained by starting the growth of polymer chain
86 from initiator molecules covalently assembled on a substrate (in
87 this case silicon wafer) by means of surface-initiated atom
88 transfer radical polymerization (SI-ATRP). ATRP is one of the
89 most versatile controlled radical polymerization techniques,
90 allowing the synthesis of polymers with well-defined
91 architectures and compositions.[16] Many ATRP initiators
92 suitable for grafting-from have been described in the literature,
93 with different surface-anchoring groups:[17] thiols and disulfides
94 are ideal for gold surfaces, and phosphonates have strong
95 affinity for oxide surfaces while dopamine-derived molecules
96 have been claimed to be suitable for virtually any kind of
97 surface.[18] However, chlorosilane and especially alkoxysilane
98 derivatives are still the most popular, thanks to their versatility,
99 ease of synthesis, and user-friendliness.[17]

100 This is the first dedicated investigation on the impact of the
101 initiator layer on the structure and properties of grafted-from
102 polymer brushes. We chose to investigate two alkoxysilane-
103 based initiators: (3-(2-bromoisobutyryl)propyl)dimethyl-
104 ethoxysilane (BIB-DMES) and (3-(2-bromoisobutyramido)-
105 propyl)triethoxysilane (BIB-APTES). They both can form
106 stable bonds with an oxide surface; however, BIB-DMES is

monofunctional, i.e., can only form one bond with the surface 107
(Figure S1a), while BIB-APTES is trifunctional and has the 108
possibility to make three bonds (Figure S1b). While the former 109
can give rise only to a monolayer, the latter can form either 110
monolayers or disordered multilayers, depending on the 111
deposition procedure. Here, by means of PAS, we show how 112
these differences are eventually reflected in the polymerization 113
kinetics and in the structure of polymer brushes obtained by 114
grafting-from. 115

■ **EXPERIMENTAL SECTION** 116

All reagents were purchased from Aldrich and used as received. Silicon 117
(100) wafers, single-polished, n type, phosphorus doped, 3−6 Ω cm, 118
with a native oxide layer ca. 1.5 nm thick, purchased from Ultrasil 119
Corporation, were cut into substrates and cleaned by immersion in a 120
3:1 v/v mixture of 98% sulfuric acid and 30% hydrogen peroxide 121
("piranha solution") at 100 °C for 1 h, rinsed extensively with water, 122
and dried with a nitrogen stream. 123

Preparation of the Initiator-Functionalized Substrates and 124
Grafting-from of PDMAEMA Brushes by SI-ATRP. In the grafting- 125
from approach to polymer brushes, two main steps are required. First, 126
the substrate is functionalized with a self-assembled layer of initiator 127
molecules, and then the initiator layer is amplified into polymer 128
brushes by a surface-initiated polymerization technique. The 129 f1
experimental process is schematized in Figure 1. 130 f1

The (3-(2-bromoisobutyryl)propyl)dimethylethoxysilane (BIB- 131
DMES) initiator was synthesized by the hydrosilylation of dimethyl- 132
ethoxysilane with allyl 2-bromoisobutyrate in the presence of 133
Karstedt's catalyst.[19] Synthesis of (3-(2-bromoisobutyramido)propyl)- 134
triethoxysilane (BIB-APTES) initiator was accomplished by reacting 3- 135
aminopropyltriethoxysilane with 2-bromoisobutyryl bromide as 136
previously described.[5] Complete synthetic procedures are available in 137
the Supporting Information. 138

Silicon and glass substrates were piranha-cleaned and then 139
immersed in a 10 mM initiator solution in anhydrous toluene, first 140
for 4 h at 55 °C and then overnight at 30 °C, eventually washed and 141
gently sonicated with toluene, acetone, and ethanol, and dried with a 142
nitrogen stream. The functionalized substrates were stored at room 143
temperature in the dark until use. 144

Poly(dimethylaminoethyl methacrylate) (PDMAEMA) brushes 145
were grown according to our previous procedure.[10] Briefly, each 146
initiator-functionalized substrate was placed in a nitrogen-purged 147
Schlenk flask and covered with 5 mL of a polymerization mixture 148

prepared as follows. In a nitrogen-purged Schlenk flask, 0.312 g (2.0 mmol) of bipyridyl and 0.144 g (1.0 mmol) of copper(I) bromide were dissolved in 6 mL of a 4:1 v/v methanol−water mixture previously degassed by bubbling nitrogen. 14 mL (83 mmol) of degassed DMAEMA was added, and the mixture was stirred under nitrogen to obtain a homogeneous solution. For polymerizations with added deactivator the polymerization mixture contained also 11 mg (0.05 mmol) of copper(II) bromide. Polymerization proceeded at 30 °C for different times to obtain brushes of increasing thickness. After polymerization, the samples were rinsed extensively with ethanol, gently sonicated in the same solvent, and dried under a nitrogen stream.

Immersion for 1 h in aqueous 0.1 M HNO_3 converted the PDMAEMA brushes in the protonated form. The brushes were then rinsed with water and dried under a nitrogen stream. For the incorporation of silver nanoparticles, the protonated brushes were immersed in a suspension of citrate-stabilized silver nanospheres for 10 min under gentle stirring. Eventually the particle-loaded brushes were washed with water, sonicated for 5 min to detach loosely bound particles, and dried under a nitrogen stream. The synthesis of silver nanoparticles has already been described in detail elsewhere.[10,20]

Positron Annihilation Spectroscopy. For the sake of concision, only PAS techniques will be described in this section. A complete and detailed description of all other characterization techniques used is available in the Supporting Information.

Doppler broadening spectroscopy (DBS) was conducted by means of the VEPAS beam, available at the LNESS facility in Como (Italy).[10] Thirty-eight values for the positron implantation energy were chosen between 0.1 and 18 keV and, for each energy value, two hyperpure Ge detectors coupled with a MCA system recorded the annihilation spectrum. The positron annihilation peak is centered at 511 keV. Its broadening is a consequence of the Doppler effect due to the electron−positron center of mass momentum respect to the laboratory frame of reference. The S-parameter is then defined as the ratio between the area in the central part of the annihilation peak, within the energy range of 511 ± 0.85 keV ($|p_I| \leq 0.456$ atomic units). The total area of the peak is taken in the range 511 ± 4.25 keV. The S-parameter corresponds to the annihilation of the positrons with the valence electrons of the material, p-Ps annihilation, or the o-Ps atoms undergoing pick-off annihilation. In the present work, the S-parameter value is an average of both detectors (weighted with the statistics of each annihilation peak area of each detector) and is normalized to one for the silicon substrate value.

Positron annihilation lifetime spectroscopy (PALS) was performed using the Monoenergetic Positron Source (MePS) at the super-conducting electron linear accelerator ELBE (Electron LINAC with high Brilliance and low Emittance) at the Helmholtz-Zentrum Dresden-Rossendorf.[21] Injection of electrons from an injector is performed through a suitable pulse repetition rate, up to 26 MHz. The incident electron beam is delivered by the superconducting electron linear accelerator ELBE at energies up to 35 MeV. The electron beam is directed toward a water-cooled tungsten bremsstrahlung converter. Electron bremsstrahlung with a continuous spectrum up to the electron beam energy is then converted by pair production into electrons and positrons inside the converter and inside a following tungsten moderator. Thermalized positrons from the moderator are being accelerated with a bias potential of +2 kV toward a conductive mesh at a few millimeters distance. Further positron transport is accomplished by a longitudinal magnetic field of 8 mT. Then, positrons are sent through a double-beam chopper which imposes a transversal electric field. Out-of-phase positrons are removed, and the beam is further longitudinally compressed with a double-slit buncher operating at a frequency of 78 MHz. A six-stage electrostatic acceleration structure follows, allowing the positron kinetic energy and thus the penetration depth inside the sample to be varied. Prior to the target the magnetic guidance system is bent by 45°, thus suppressing positrons reflected from the sample and bounced by the accelerator field to impact again onto the sample. The sample station is kept at a high potential of up to 20 kV. About 3 cm behind the sample a μ-metal shielded BaF_2 scintillation detector is employed for annihilation lifetime measurements. The timing reference is derived from the precision master oscillator of the superconducting accelerator and is phase-matched to the electron bunches of the beam. A magnetic beam transport system guides positrons to the samples under investigation. A dedicated chopper/buncher system is used to maintain a high timing resolution for depth-dependent annihilation lifetime studies in thin films. Further details of the apparatus can be found in a previous reference.[22] The signal-to-noise ratio is above 10^4 while lifetime resolutions of up to 230 ps fwhm have been obtained. The time resolution of the system was in the range 230 ps (at 0.5 keV)− 700 ps (at 6 keV), according to the energy of the implanted positrons. The count rate of the system was about 10^4 Hz. For each incident energy, spectra with 5×10^6 counts for each lifetime spectrum in about 10 min were acquired.

RESULTS AND DISCUSSION

Characterization of the Initiator Layers. The initiator layers have been characterized using a wide range of surface analytical techniques (water contact angle, spectroscopic ellipsometry, X-ray photoelectron spectroscopy, atomic force microscopy) and the information combined to obtain a clear picture of their structure.

The water contact angle θ_w of initiator-functionalized surfaces significantly increased ($\theta_w = 75 \pm 3°$ for both initiators) from the starting highly hydrophilic piranha-treated silicon surface ($\theta_w = 0°$), in accordance with literature findings.[23] A first estimate of the initiator surface coverage was obtained using the Israleachvili−Gee equation (eq 1).[24] This equation correlates the equilibrium contact angle of a chemically heterogeneous surface to the surface coverage of the different molecules on the surface and predicts an increase in water contact angle with an increase in surface coverage of small hydrophobic molecules (in this case the initiator molecules):

$$[1 + \cos(\theta_{obs})]^2 = f_1[1 + \cos(\theta_1)]^2 + f_2[1 + \cos(\theta_2)]^2$$
$$f_1 + f_2 = 1$$

(1)

The water contact angle of a surface completely covered with initiator molecules ($f_1 = 1$) is assumed to be $\theta_1 = 80°$ according to the maximum value reported in the literature for ordered monolayers of bromoalkylsilanes,[25,26] while the water contact angle of a completely hydrophilic silicon wafer surface ($f_2 = 1$) is $\theta_2 = 0°$. The obtained high value $f_1 = 0.9$ suggests the formation of homogeneous initiator layers.

The thickness of the initiator layers was determined using spectroscopic ellipsometry. This allowed also to discriminate between mono- and multilayer formation. The measured thickness values (0.7 ± 0.1 nm for BIB-DMES, 1.5 ± 0.2 nm for BIB-APTES) were in good agreement with previously reported values for densely grafted silane-based initiator layers.[27] Knowing the thickness h, the surface density σ_I of initiator molecules was calculated according to eq 2:

$$\sigma_I = \frac{N_A h \rho}{M_n}$$

(2)

where ρ is the density of the silane coupling agent (assuming a uniform, well-packed, fully extended layer with a density equal to that measured for the bulk siloxane: $\rho_{BIB-DMES} = 1.12$ g cm^{-3}; $\rho_{BIB-APTES} = 1.17$ g cm^{-3}), M_n is the molecular weight of the completely hydrolyzed, Si−OH-terminated siloxanes ($M_{n,BIB-DMES} = 283$ g mol^{-1}; $M_{n,BIB-APTES} = 286$ g mol^{-1}) and N_A is Avogadro's number. In this way, surface density values of

Table 1. Atomic Composition (Expressed as atomic % ± 10%) and Calculated Elemental Ratios of Initiator-Functionalized Surfaces As Determined by XPS

initiator	O	C	Si	N	Br	N/C (theor)	Br/C (theor)	N/Br (theor)
BIB-DMES	43.3	21.1	35.5		0.21		0.01 (0.11)	
BIB-APTES	38.0	24.6	34.5	2.6	0.33	0.11 (0.14)	0.013 (0.14)	0.13 (1)

1.6 molecules nm^{-2} for BIB-DMES and of 4 molecules nm^{-2} for BIB-APTES were obtained. Densely packed self-assembled monolayers of alkylsilanes on silicon substrates typically have values within the range of ∼1.5−3 molecules nm^{-2}, suggesting that while BIB-DMES forms a dense monolayer, BIB-APTES generates more likely a bilayer.

X-ray photoelectron spectroscopy provided a semiquantitative elemental analysis of the surfaces modified with the two ATRP initiators. The results, listed in Table 1, provide the confirmation that both initiators were successfully grafted on the silicon surface.

The morphological quality of the initiator-functionalized substrates was assessed with AFM (Figure S2). The surface roughness increased only slightly from the piranha-cleaned silicon substrate (rms 0.17 nm) to a BIB-APTES functionalized substrate (rms 0.26 nm) but significantly increased for a BIB-DMES functionalized substrate (rms 0.71 nm) due to the presence of structures resulting from an island-type growth of the monolayer.[28]

PDMAEMA Brushes. Surface-initiated atom transfer radical polymerization (SI-ATRP) is one of the most versatile controlled radical polymerization techniques, thanks especially to its tolerance to water and oxygen, its compatibility with a wide range of functional monomers, and the possibility of conducting the polymerization at ambient temperature. The mechanism of SI-ATRP is based on the reversible formation of radicals by halogen atom abstraction from a surface-attached alkyl halide (typically a secondary or tertiary bromide) by a copper(I)−ligand complex. The latter breaks the C−Br bond of the initiator, and the resulting carbon−carbon-centered radical attacks a monomer molecule, thereby starting the chain growth from the substrate surface. At the same time, copper(I) is oxidized to copper(II). Since this process is reversible, Cu(II) acts as a deactivator, reducing the overall concentration of active radicals and thus the occurrence of termination events.

Despite the great amount of research that has been performed on SI-ATRP-made PDMAEMA brushes, little attention has been paid to the impact of initiator type on the polymerization kinetics and on the characteristics of the resulting brushes. From the polymerization kinetics shown in Figure S3a it is apparent that PDMAEMA chains stopped growing from BIB-DMES earlier compared to those growing from BIB-APTES, suggesting that irreversible chain termination events were more frequent for the monofunctional initiator layer. Such behavior is not strictly dependent on the monomer or on the polymerization conditions, since it was observed for other monomers (methyl methacrylate, MMA, and styrene, Sty) polymerized with ATRP using the same (for MMA) and even different conditions (for Sty) (Figure S4). A stronger evidence for such behavior was obtained by repeating the polymerization in the presence of added deactivator (5 mol % $CuBr_2$), a strategy which is known to increase control of the polymerization process by suppressing the rate of irreversible radical termination.[29] The effect of added deactivator was found to be dramatically different for the two initiators: in presence of $CuBr_2$, the growth of brushes from BIB-APTES showed a linear increase in thickness as a function of polymerization time, while the kinetics of brushes grown from BIB-DMES was not affected (Figure S3b).

X-ray reflectivity (XRR) was used to determine the thickness, density, interface roughness, and surface roughness of the PDMAEMA brushes. XRR gave an evidence of the good quality of the initiator layer by showing a smooth, high-quality substrate/brush interface with a mean roughness value ≤0.3 nm for all samples. The results, summarized in Table S1, showed also that the average surface roughness is higher for brushes grown from BIB-DMES compared to the brushes grown from BIB-APTES, suggesting the latter ones to be more ordered.

Using the thickness h and density ρ values, the surface coverage Γ of PDMAEMA brushes was calculated. It is assumed that when the brush is measured in air, the brush is fully collapsed and assumes a slablike conformation, with a "dry" thickness h. For a uniform brush layer, this dry thickness is equal to the volume of polymer per unit area covering the substrate and is proportional to the mass of grafted material (eq 3).

$$\Gamma = h\rho \qquad (3)$$

The representation of Γ versus the polymerization time shows a good correlation (Figure S5), suggesting that the synthesis of polymer brushes was controlled. The experimental determination of brushes' molecular weight is extremely challenging; however, it is possible to calculate the minimum chain M_n using eq 4, a modified version of eq 1, by assuming that all initiator sites induce polymerization and grow with an identical rate, i.e., providing the polymer monolayer to be in the brush regime without a significant density gradient along the chain:
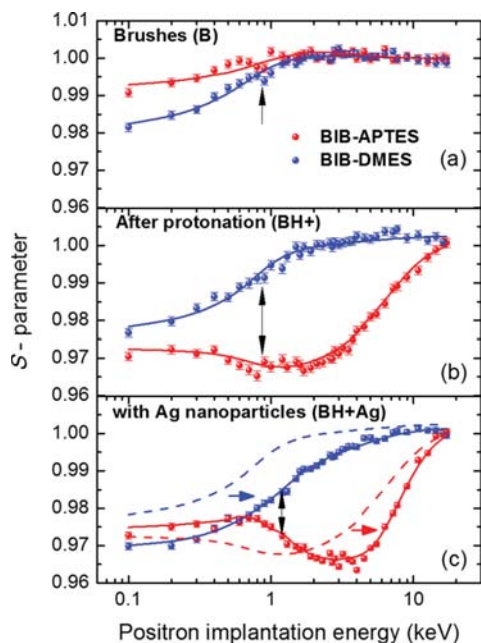
$$M_n = \frac{N_A \Gamma}{\sigma_I} \qquad (4)$$

where M_n is the average chain molecular weight, Γ is the polymer surface coverage, and σ_I is the surface density of initiator molecules. However, the fraction of initiator molecules that induces simultaneous polymer growth is generally less than unity,[30] due to factors, such as the monomer size, which affect the initiator efficiency due to steric hindrance of the active sites.[31] Thus, the calculated M_n values listed in Table S1 represent a lower limit, and a grafting density of 0.5 chains nm^{-2} was chosen to perform the calculations. It should be noted that the calculated M_n values for the brushes grown from the BIB-DMES initiator are an order of magnitude higher compared to those for brushes grown from the BIB-APTES initiator. This effect could be directly related to the different density of surface initiating sites: on flat substrates, the efficiency of chain initiation and propagation is obstructed by the dense packing of chains. Thus, for equal thicknesses, brushes grown from the BIB-APTES initiator would be denser and more stretched compared to those grown from the BIB-DMES initiator. AFM showed a higher density of defects and pinholes for the brushes obtained using BIB-DMES as the

initiator (Figure S6), supporting the conclusion that brushes obtained from BIB-APTES are more ordered.

Silver nanoparticles were then incorporated into protonated PDMAEMA brushes, following our previously reported protocol.[10] Successful incorporation of silver nanoparticles in the brushes was demonstrated by UV–vis absorption spectroscopy. A broad peak, centered at around 500 nm, corresponding to the surface plasmon resonance of embedded silver nanoparticles (Figure S7) was found for all samples. Scanning electron microscopy (Figure S8) revealed the presence of silver nanoparticles as bumps in the originally flat polymer surface, and backscattered electron analysis confirmed that the particles were truly embedded inside the brushes instead than just decorating the surface.

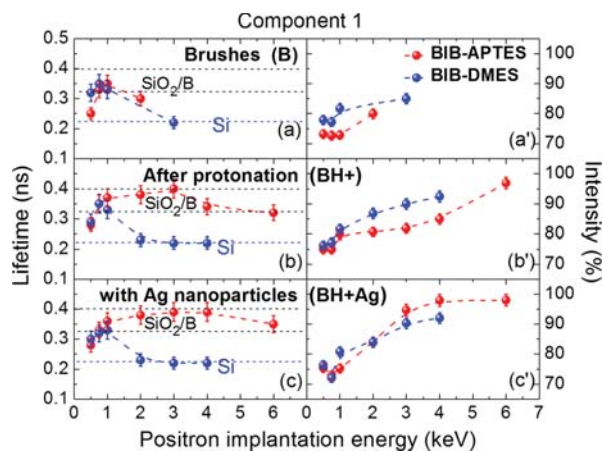**Positron Annihilation Spectroscopy.** A total of six samples were analyzed by means of positron annihilation spectroscopy. The **B** samples were as-prepared brushes. The two **BH+** samples were protonated by immersion in dilute nitric acid while the **BH+Ag** samples were first protonated and then immersed in an aqueous suspension of silver nanoparticles to allow the uptake of the latter. Two samples, one for each kind of initiator, were prepared and analyzed.

The S-parameter evolution as a function of the positron implantation energy E for PDMAEMA brushes, shown in Figure 2a, is very similar irrespective of the initiator used. At low implantation energy, the positrons tend to diffuse to the surface, thus influencing the information given by the S-parameter. However, the small difference observed in Figure 2a for $E \leq 1$ keV would be linked with a difference in the morphology of the brushes. The positron lifetime of the first component in Figure 3a for the same range of implantation energy ($E \leq 1$ keV) is around 250−350 ps, with a relative

Figure 3. Positron lifetime and the relative intensity of the first component in samples of PDMAEMA brushes obtained with two different initiators, BIB-APTES and BIB-DMES, plotted against the positron implantation energy: (a) and (a′) as-made (**B**), (b) and (b′) after protonation (**BH+**), and (c) and (c′) after silver nanoparticles loading (**BH+Ag**). The lines through the experimental data are a guide for the eye. The horizontal dashed lines represent the positron lifetime in Si and a range of values for annihilation at the interface brushes/Si substrate and into the brushes (see text).

intensity of 70−80%. This is attributed to a combined effect of the positrons that annihilate into the brushes microstructure and the parapositronium annihilation in two γ-rays. The second and third components for $E \leq 1$ keV in Figure 4a are instead related to free volumes between polymer chains and nanometric cavities between brushes, respectively. The lifetime values of these components tend to be similar but slightly higher for the BIB-DMES-initiated brushes compared to the BIB-APTES-initiated ones. The free volume diameters between
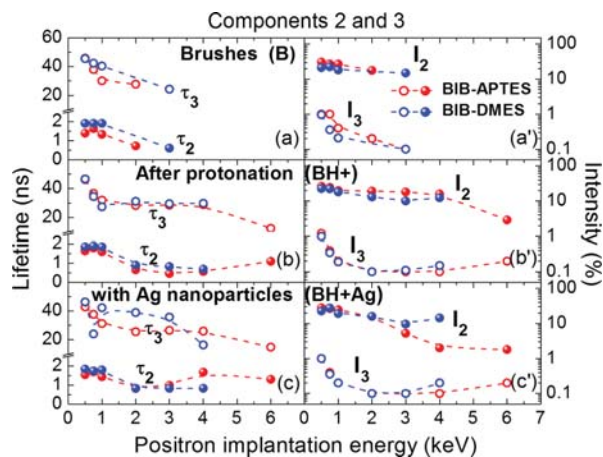

Figure 2. Normalized S-parameter as a function of the positron mean implantation energy in samples of PDMAEMA brushes obtained with two different initiators, BIB-APTES and BIB-DMES: (a) as-made (**B**), (b) after protonation (**BH+**), and (c) after loading of silver nanoparticles (**BH+Ag**) (dashed curves reproduce **BH+**). The lines through the experimental data represent the results of a best-fit procedure obtained with VEPFIT. The vertical black arrows show the estimated average implantation depth equivalent to the expected position of the interface brushes/Si substrate.

Figure 4. Positron lifetime and the relative intensity of the second and third components in samples of PDMAEMA brushes obtained with two different initiators, BIB-APTES and BIB-DMES, plotted against the positron implantation energy: (a) and (a′) as-made (**B**), (b) and (b′) after protonation (**BH+**), and (c) and (c′) after loading of silver nanoparticles (**BH+Ag**). The lines through the experimental data are just a guide for the eye. The experimental error bars are within the symbols.

polymer chains, calculated using the extended Tao−Eldrup model,[32] are 0.57 and 0.50 nm respectively for the BIB-DMES-initiated and for the BIB-APTES-initiated brushes. The intensity of the third component is very weak (≤1%), suggesting a low density of cavities between brushes of about 2.5−3 nm in diameter. The S-parameter for higher implantation energies ($E \geq 2$ keV in Figure 2a) tends to 1; i.e., positrons annihilate into the Si substrate. The lifetime information on Figure 3a corroborates this finding in the case of the BIB-DMES-initiated brushes, taking into account that the positron lifetime in Si is 220 ps.[33]

The effect of the initiator is more clearly revealed, as a difference between the evolutions of the S-parameter, after protonation of the brushes (Figure 2b, samples **BH+**). Protonation, i.e., the acid−base reaction of nitric acid with the PDMAEMA tertiary amine groups, does not alter the mass density of the brushes. For the BIB-APTES-initiated brushes, the S-parameter falls within a broad minimum extended up to ∼2 keV. Considering the characteristics of the studied material, it would be expected that most of the positrons annihilates into the Si substrate for implantation energies in the range of 2−3 keV as observed for the BIB-DMES-initiated brushes, where the S-parameter tends to one. In order to understand the difference between the brushes grown with different initiators, the VEPFIT program has been used for the data fitting.[34] A layered model was adopted, consisting of a surface, a brush layer, an interface and a silicon substrate. The free parameters of the model,[10] for each layer, are the S-parameter value, the positron diffusion length, the electric field (if present), and the layer density. The model is implemented with a recursive procedure that gives a best fit of the measured S-parameter evolution and is based on the solution of the diffusion equation for the implanted positrons in each layer of the heterostructure, considering the energy-dependent positron implantation profiles. The S-parameter data taken for the protonated BIB-APTES-initiated brushes can be successfully modeled by VEPFIT only if an electric field is included into the substrate and in the brushes themselves. A detailed description is provided in the Supporting Information (pp S5−S7). This electric field does not affect the positron implantation profiles at high energies, but when the positrons reach the thermal equilibrium with the material, its presence becomes relevant acting on the positrons as a drifting force. This is especially true for the Si substrate, where positrons diffuse for long distances (200−230 nm without field in intrinsic and n-doped Si as in the studied case[35]). After protonation, the electric field vector points outward the brush surface. Thereby, positrons implanted and thermalized into Si are affected by the presence of this field and are strongly oriented toward the brushes/Si interface. The interface is modeled as a thin film (∼1−2 nm) with a very low positron diffusion length (≤1 nm, similar to a previous reference[36]), i.e., highly trapping for positrons. Physically, this interface is equivalent to the native oxide on the Si substrate and possibly also to the initiator layer. Positrons migrating from silicon could also overstep the interface and reach the brushes rich of polarized chains.

This picture is coherent with the results observed for the first lifetime component in Figure 3b. The positron lifetime for implantation energies ≥3 keV indeed tends to the lifetime in Si (∼220 ps)[33] with a relative intensity ∼90% for the BIB-DMES-initiated brushes. Instead, in the case of BIB-APTES-initiated brushes, the lifetime tends to 320−400 ps, which is attributed to the lifetime of the first component at the brushes/SiO$_2$

interface and inside the brushes. The second lifetime component (Figure 4b) indicates that for implantation energies lower than 4 keV between 10% and 30% of the positrons form positronium and annihilate into the free volumes ≤0.5 nm in diameter. Instead, the nanometric cavities between brushes with higher diameter of 2.5−3 nm associated with the third component (Figure 4b) are practically negligible, the intensity of this component being less than 1%. A component with such a long lifetime is absent in the spectra of polymers investigated in the usual conditions (that is, when positrons annihilate in the bulk). On the contrary, in our data it is present for pristine and protonated samples as well as after loading of silver nanoparticles. This suggests that the big cavities responsible of the long lifetime are mainly found in the proximity of the surface, where the distances among brushes can be higher than in the layers below, due to their flexibility. This interpretation is supported also by the systematic decrease of intensity at higher positron implantation energies. Indeed, the more energetic the particles, the less the fraction of them captured near the surface, with consequent smaller probability of o-Ps formation in the cavities.

It is proposed that the nature of the electric field observed after protonation in the BIB-APTES sample is related to the polarization and orientation of the brushes. PDMAEMA is a weak polyelectrolyte with pK_a ∼ 7, which makes its tertiary amine groups easily protonated by immersion in acid solutions. During the protonation step, the reaction of nitric acid with the tertiary amine groups of PDMAEMA generates electric dipoles along each polymer chain with the positive charges located on the protons and the negative ones on the nitrate counterions. In the case of the BIB-APTES-initiated brushes, the VEPFIT model reproduces the experimental results only if the field is present in the brushes region and it induces a depletion zone (with a net electric field) into the Si substrate.[37] The width of the depletion zone depends of the doping density of the substrate, which in this case is of the order of 1 μm.[38] The absolute value of the field indicated by the fitting program is 300 ± 100 kV cm^{-1}, which corresponds to a net potential on the brushes surface of about 0.5 V. On the other hand, the data obtained for the BIB-DMES-initiated brushes were successfully modeled without the introduction of an electric field. The VEPFIT model indicates that the electric field, if it is present at all, should be 1 order of magnitude lower compared to the BIB-APTES-initiated brushes (within the estimated determination error ∼±50 kV cm^{-1}). This remarkable difference could be due to a different orientation of the polymer chains, which should be less ordered and more randomly oriented in the BIB-DMES-initiated brushes compared to the BIB-APTES-initiated ones as shown qualitatively in Figure S9.

The positive charges on protonated PDMAEMA brushes facilitate the incorporation of premade dipolar silver nano-particles with a negative surface charge[39] by means of a simple immersion step. When silver nanoparticles (AgNPs) are loaded into the protonated brushes, the S-parameter evolution in Figure 2c (samples **BH+Ag**) is shifted to the right, i.e., to higher implantation energies. Following the VEPFIT model, another consequence of nanoparticle incorporation is an increase in the density of the brushes layer, as shown in Table 2. The introduction of an electric field was necessary to reproduce the evolution of the S-parameter for the nano-particle-loaded BIB-APTES-initiated brushes (Figure 2c). Compared to the protonated brushes, the field here is more intense and reaches values of the order of 900 ± 200 kV cm^{-1}

Table 2. Summary of the Results Obtained for the Different Brushes Samples by Fitting Positron Annihilation Data with the VEPFIT Model

sample	protonation	thickness[a] (nm)	density (g cm^{-3})	Ag filling (%)	fit variance χ^2/DOF
B (BIB-APTES)	no	37	1.5 ± 0.2	0	1.73
B (BIB-DMES)	no	29	1.5 ± 0.2	0	1.5
BH+ (BIB-APTES)	yes	20	1.5 ± 0.2	0	1.12
BH+ (BIB-DMES)	yes	29	1.5 ± 0.2	0	1.5
BH+Ag (BIB-APTES)	yes	27	2.1 ± 0.2	6 ± 3	1.52
BH+Ag (BIB-DMES)	yes	29	2.5 ± 0.3	7 ± 4	1.16

[a]Measured by X-ray reflectivity.

(corresponding to a potential on the brushes surface slightly higher than 1 V), which is of the same order of magnitude of the electric field recently calculated for polyelectrolyte brushes.[40] The increase of the electric field is linked to the incorporation of the Ag nanoparticles. When the silver particles are incorporated in the brushes, the negatively charged citrate molecules on their surface are neutralized by an acid–base reaction with the positively charged protonated amine groups. The now free surface of the particles is stabilized by the tertiary amine groups through a dipolar interaction with the lone pair of the nitrogen atom.[41] The particles' dipoles tend to be oriented in the same direction of the protonated chains' dipoles, increasing the overall electrostatic energy. This effect increases the field into the depletion region at the substrate, as mentioned before for the more oriented BIB-APTES-initiated brushes. Evidence for the presence of an electric field was not observed in the case of BIB-DMES-initiated brushes after loading of Ag nanoparticles (within the estimated determination error ~±100 kV cm^{-1}).

The density values listed in Table 2 suggest that for both BIB-DMES- and BIB-APTES-initiated brushes the percentage of loaded silver nanoparticles is similar and is between 5 and 10% (within the experimental error). Since the fraction of positrons implanted into the nanoparticles can easily diffuse in the metal matrix, eventually reaching the particle's surface (which is richer in defects) and the brushes, or forms positronium which subsequently annihilates, the presence of Ag nanoparticles is observed indirectly from the point of view of the positron annihilation sites, in accordance with our previous interpretation.[10]

■ CONCLUSIONS

Positron annihilation spectroscopy (PAS) provides, for the first time, a clear evidence of the impact of the initiator layer on the characteristics of polymer brushes obtained by the grafting-from approach. Silicon surface was functionalized with two different silane-based initiators: monofunctional (BIB-DMES) and trifunctional (BIB-APTES). Both the initiator-modified surfaces and the poly(dimethylaminoethyl methacrylate) (PDMAEMA) brushes obtained by surface-initiated atom transfer radical polymerization (SI-ATRP) were thoroughly characterized with conventional surface analysis techniques.

The results were correlated with those obtained by PAS. Thanks to the pH-responsive properties of PDMAEMA, the brushes could be easily modified by protonation and subsequent incorporation of silver nanoparticles and the resulting effects on positrons' behavior and on positronium formation were successfully evaluated. The most dramatic differences were found, after the protonation step, for the BIB-APTES-initiated brushes. This might be related to the generation of an electric field thanks to the high density of polarized amine groups on the polymer chains. The intensity of the electric field increased after the incorporation of Ag nanoparticles and clearly affected the behavior of implanted positrons. The absence of such electric field in the protonated BIB-DMES-initiated brushes would suggest a lower degree of homogeneity compared to BIB-APTES-initiated brushes, which, being more tightly packed and oriented in the direction perpendicular to the substrate surface, can generate a stronger electric field.

Our unprecedented results constitute a solid proof that positron annihilation spectroscopy has much to contribute to the study of polymer brushes.

■ ASSOCIATED CONTENT

ⓈSupporting Information

The Supporting Information is available free of charge on the ACS Publications website at DOI: 10.1021/acs.macro-mol.7b00953.

> Complete description of experimental procedures; additional data and figures (PDF)

■ AUTHOR INFORMATION

Corresponding Authors
*E-mail: gp4779@gmail.com (G.P.).
*E-mail: giovanni.consolati@polimi.it (G.C.).

ORCID
Guido Panzarasa: 0000-0003-1044-0491

Present Address
G.P.: Empa Materials Science and Technology, Laboratory for Biomimetic Membranes and Textiles, Lerchenfeldstrasse 5, 9014 St. Gallen, Switzerland.

Notes
The authors declare no competing financial interest.

■ REFERENCES

(1) Jean, Y. C.; Van Horn, J. D.; Hung, W. S.; Lee, K. R. Perspective of Positron Annihilation Spectroscopy in Polymers. *Macromolecules* **2013**, *46*, 7133−7145.

(2) Dlubek, G.; Kilburn, D.; Bondarenko, V.; Pionteck, J.; Krause-Rehberg, R.; Alam, M. A. Positron Annihilation: A Unique Method for Studying Polymers. *Macromol. Symp.* **2004**, *210*, 11−20.

(3) Gidley, D. W.; Peng, H.-G.; Vallery, R. S. Positron Annihilation As a Method To Characterize Porous Materials. *Annu. Rev. Mater. Res.* **2006**, *36*, 49−79.

(4) Azzaroni, O. Polymer Brushes Here, There, and Everywhere: Recent Advances in Their Practical Applications and Emerging

Opportunities in Multiple Research Fields. *J. Polym. Sci., Part A: Polym. Chem.* 2012, 50 (16), 3225−3258.

(5) Panzarasa, G.; Soliveri, G.; Sparnacci, K.; Ardizzone, S. Patterning of Polymer Brushes Made Easy Using Titanium Dioxide: Direct and Remote Photocatalytic Lithography. *Chem. Commun.* 2015, 51, 7313−7316.

(6) Panzarasa, G.; Soliveri, G.; Ardizzone, S. Crafting Positive/Negative Patterns and Nanopillars of Polymer Brushes by Photocatalytic Lithography. *Colloids Surf., A* 2016, 506, 833−839.

(7) Panzarasa, G.; Soliveri, G.; Pifferi, V. Tuning the Electrochemical Properties of Silicon Wafer by Grafted-from Micropatterned Polymer Brushes. *J. Mater. Chem. C* 2016, 4, 340−347.

(8) Panzarasa, G.; Dübner, M.; Pifferi, V.; Soliveri, G.; Padeste, C. ON/OFF Switching of Silicon Wafer Electrochemistry by pH-Responsive Polymer Brushes. *J. Mater. Chem. C* 2016, 4, 6287−6294.

(9) Senaratne, W.; Andruzzi, L.; Ober, C. Self-Assembled Monolayers and Polymer Brushes in Biotechnology: Current Applications and Future Perspectives. *Biomacromolecules* 2005, 6, 2427−2448.

(10) Panzarasa, G.; Aghion, S.; Soliveri, G.; Consolati, G.; Ferragut, R. Positron Annihilation Spectroscopy: A New Frontier for Understanding Nanoparticle- Loaded Polymer Brushes. *Nanotechnology* 2016, 27 (2), 02LT03.

(11) Weber, M. H.; Kynn, K. G. *Principles and Applications of Positron and Positronium Chemistry*; Jean, Y. C., Mallon, P. E., Schrader, D. M., Eds.; World Scientific: Singapore, 2003.

(12) Dlubek, G. P. P. *Polymer Physics. From Suspensions to Nanocomposites and Beyond*; Utracki, L. A., Jamieson, A. M., Eds.; John Wiley & Sons: Singapore, 2010.

(13) De Smedt, S. C.; Demeester, J.; Hennink, W. E. Cationic Polymer Based Gene Delivery Systems. *Pharm. Res.* 2000, 17, 113−126.

(14) Christau, S.; Genzer, J.; von Klitzing, R. Polymer Brush/Metal Nanoparticle Hybrids for Optical Sensor Applications: From Self-Assembly to Tailored Functions and Nanoengineering. *Z. Phys. Chem.* 2015, 229, 1089−1117.

(15) Thomas, M.; Gajda, M.; Amiri Naini, C.; Franzka, S.; Ulbricht, M.; Hartmann, N. Poly(N,N-Dimethylaminoethyl Methacrylate) Brushes: PH-Dependent Switching Kinetics of a Surface-Grafted Thermoresponsive Polyelectrolyte. *Langmuir* 2015, 31, 13426−13432.

(16) Matyjaszewski, K.; Xia, J. Atom Transfer Radical Polymerization. *Chem. Rev.* 2001, 101, 2921−2990.

(17) Barbey, R.; Lavanant, L.; Paripovic, D.; Schüwer, N.; Sugnaux, C.; Tugulu, S.; Klok, H.-A. Polymer Brushes via Surface-Initiated Controlled Radical Polymerization: Synthesis, Characterization, Properties, and Applications. *Chem. Rev.* 2009, 109 (11), 5437−5527.

(18) Kuang, J.; Messersmith, P. B. Universal Surface-Initiated Polymerization of Antifouling Zwitterionic Brushes Using a Mussel-Mimetic Peptide Initiator. *Langmuir* 2012, 28, 7258−7266.

(19) Ohno, K.; Akashi, T.; Huang, Y.; Tsujii, Y. Surface-Initiated Living Radical Polymerization from Narrowly Size-Distributed Silica Nanoparticles of Diameters Less than 100 Nm. *Macromolecules* 2010, 43, 8805−8812.

(20) Panzarasa, G. Shining Light on Nanochemistry Using Silver Nanoparticle-Enhanced Luminol Chemiluminescence. *J. Chem. Educ.* 2014, 91 (5), 696−700.

(21) Gabriel, F.; Gippner, P.; Grosse, E.; Janssen, D.; Michel, P.; Prade, H.; Schamlott, A.; Seidel, W.; Wolf, A.; Wünsch, R. The Rossendorf Radiation Source ELBE and Its FEL Projects. *Nucl. Instrum. Methods Phys. Res., Sect. B* 2000, 161−163, 1143−1147.

(22) Wagner, A.; Anwand, W.; Attallah, A. G.; Dornberg, G.; Elsayed, M.; Enke, D.; Hussein, A. E. M.; Krause-Rehberg, R.; Liedke, M. O.; Potzger, K. Positron Annihilation Lifetime Spectroscopy at a Superconducting Electron Accelerator. *J. Phys.: Conf. Ser.* 2017, 791 (1), 012004.

(23) Retsch, M.; Walther, A.; Loos, K.; Müller, A. H. E. Synthesis of Dense Poly(acrylic Acid) Brushes and Their Interaction with Amine-Functional Silsesquioxane Nanoparticles. *Langmuir* 2008, 24, 9421−9429.

(24) Israelachvili, J.; Gee, M. Contact Angles on Chemically Heterogeneous Surfaces. *Langmuir* 1989, 5, 288−289.

(25) Kurth, D. G.; Bein, T. Surface Reactions on Thin Layers of Silane Coupling Agents. *Langmuir* 1993, 9, 2965−2973.

(26) Li, L.; Zhu, Y.; Li, B.; Gao, C. Fabrication of Thermoresponsive Polymer Gradients for Study of Cell Adhesion and Detachment. *Langmuir* 2008, 24, 13632−13639.

(27) Barbey, R.; Klok, H. A. Room Temperature, Aqueous Post-Polymerization Modification of Glycidyl Methacrylate-Containing Polymer Brushes Prepared via Surface-Initiated Atom Transfer Radical Polymerization. *Langmuir* 2010, 26, 18219−18230.

(28) Welch, M. E.; Ober, C. K. Characterization of Polymer Brush Membranes via HF Etch Liftoff Technique. *ACS Macro Lett.* 2013, 2, 241−245.

(29) Matyjaszewski, K. Atom Transfer Radical Polymerization (ATRP): Current Status and Future Perspectives. *Macromolecules* 2012, 45, 4015−4039.

(30) Jones, D. M.; Brown, A.; Huck, W. T. S. Surface-Initiated Polymerizations in Aqueous Media: Effect of Initiator Density. *Langmuir* 2002, 18 (13), 1265−1269.

(31) Malham, I. B.; Bureau, L. Density Effects on Collapse, Compression, and Adhesion of Thermoresponsive Polymer Brushes. *Langmuir* 2010, 26, 4762−4768.

(32) Dull, T. L.; Frieze, W. E.; Gidley, D. W.; Sun, J. N.; Yee, A. F. Determination of Pore Size in Mesoporous Thin Films from the Annihilation Lifetime of Positronium. *J. Phys. Chem. B* 2001, 105, 4657−4662.

(33) Dannefaer, S.; Mascher, P.; Kerr, D. Monovacancy Formation Enthalpy in Silicon. *Phys. Rev. Lett.* 1986, 56 (20), 2195−2198.

(34) Van Veen, A.; Schut, H.; De Vries, J.; Hakvoort, R. A.; Ijpma, M. R. Analysis of Positron Profiling Data by Means of "VEPFIT". *AIP Conf. Proc.* 1991, 218, 171−198.

(35) Bauer-Kugelmann, W.; Duffy, J. A.; Störmer, J.; Kögel, G.; Triftshäuser, W. Diffusivity and Surface Transition Rate of Positrons in Crystalline Silicon as a Function of Dopant Concentration. *Appl. Surf. Sci.* 1997, 116, 231−235.

(36) Brusa, R. S.; Karwasz, G. P.; Mariotto, G.; Zecca, A.; Ferragut, R.; Folegati, P.; Dupasquier, A.; Ottaviani, G.; Tonini, R. Structural Evolution in Ar+ Implanted Si-Rich Silicon Oxide. *J. Appl. Phys.* 2003, 94, 7483−7492.

(37) Guijarro, N.; Prévot, M. S.; Sivula, K. Surface Modification of Semiconductor Photoelectrodes. *Phys. Chem. Chem. Phys.* 2015, 17, 15655−15674.

(38) Boyle, W. S.; Smith, G. E. Charge Coupled Semiconductor Devices. *Bell Syst. Technol. J.* 1970, 49, 587−593.

(39) Soliveri, G.; Pifferi, V.; Panzarasa, G.; Ardizzone, S.; Cappelletti, G.; Meroni, D.; Sparnacci, K.; Falciola, L. Self-Cleaning Properties in Engineered Sensors for Dopamine Electroanalytical Detection. *Analyst* 2015, 140, 1486−1494.

(40) He, Z.; Xie, W. J.; Liu, Z.; Liu, G.; Wang, Z.; Gao, Y. Q.; Wang, J. Tuning Ice Nucleation with Counterions on Polyelectrolyte Brush Surfaces. *Sci. Adv.* 2016, 2 (June), e1600345−e1600345.

(41) Cure, J.; Coppel, Y.; Dammak, T.; Fazzini, P. F.; Mlayah, A.; Chaudret, B.; Fau, P. Monitoring the Coordination of Amine Ligands on Silver Nanoparticles Using NMR and SERS. *Langmuir* 2015, 31, 1362−1367.